JOURNAL OF SOLID STATE CHEMISTRY 108, 59–67 (1994)

Oxygen-Defect Geometry in Oxygen-Rich $La_2Co_xCu_{1-x}O_{4+\delta}$ Layered Oxides

Alexandros Lappas and Kosmas Prassides[1]

School of Chemistry and Molecular Sciences, University of Sussex, Brighton BN1 9QJ, United Kingdom

Received February 16, 1993; accepted April 22, 1993

The structural properties of the $La_2Co_xCu_{1-x}O_{4+\delta}$ ($x = 0.25$, 0.75) series have been studied by powder neutron diffraction. Excess oxygen is accommodated as an O^{2-} ion in the interstitial space defined by the lanthanide bilayers and leads to the displacement of some of the neighboring apical oxygens of the $(Cu,Co)O_6$ octahedra from their normal lattice sites. The rigid tilt of the metal–oxygen octahedral units is, however, suppressed in the Co-rich system and the *Fmmm* space group is adopted. The Cu-rich compound is found to remain isostructural with the parent La_2CuO_4 system (space group *Bmab*). The defect occupies a unique site in the $x = 0.25$ system but is equally shared between two symmetry-equivalent positions for $x = 0.75$.

INTRODUCTION

The unifying structural feature of the high-T_c cuprate perovskites is the presence of CuO_2 layers, formed by corner-sharing square CuO_4 units. These layers are present in both hole- and electron-doped superconductors and are part of either strongly elongated octahedral CuO_6 units (O/*T* phases, $La_{2-x}Sr_xCuO_{4-\delta}$) (1–3), or square-pyramidal CuO_5 units (*T** phases, $Nd_{2-x-y}Ce_xSr_yCuO_{4-\delta}$) (4), or square-planar CuO_4 units (*T'* phases, $Nd_{2-x}Ce_xCuO_{4-\delta}$) (5–7). Changes in the formal Cu oxidation state and the filling of the conduction band can be achieved through either chemical doping of the lanthanide bilayers (e.g., Sr^{2+}, Ce^{4+}) or oxygen nonstoichiometry ($\delta \neq 0$). Superoxygenated $La_2CuO_{4+\delta}$ has been found to be superconducting with $T_c \approx 40$ K (8, 9), in sharp contrast to stoichiometric La_2CuO_4 which is an antiferromagnetic insulator (2). As a result, the structural properties of oxygen-rich cuprates and related oxides have attracted considerable interest, focusing on the pivotal role of oxygen stoichiometry in determining the structural, electronic, and conducting properties of these oxides.

Superconducting $La_2CuO_{4+\delta}$ shows little variation in the transition temperature with changes in δ. Using powder neutron diffraction measurements, Jorgensen *et al.* (10) have attributed this observation to the presence of two orthorhombic phases with nearly identical stoichiometries below 320 K: one has virtually no excess oxygen and is insulating (space group *Bmab*), while the other is oxygen rich and superconducting (space group *Fmmm*). Varying δ only changes the relative fractions of the superconducting and insulating phases. A miscibility gap was identified at $\delta \approx 0.08$. The existence of similar phase separation behavior resulting from segregation of interstitial oxygen defects was also observed in the $La_2NiO_{4+\delta}$ series (11). Furthermore, the excess interstitial oxygen, located between adjacent LaO layers near the $(\frac{1}{4}, \frac{1}{4}, \frac{1}{4})$ site, appears to adopt the same structure in both the cuprate and nickelate systems (10–12). It corresponds to a charged defect, and is tetrahedrally coordinated to four La^{3+} ions with the four neighboring oxygens being displaced from their normal positions. A different type of oxygen defect has been postulated to exist in lightly overdoped $La_{1.84}Sr_{0.16}CuO_{4.019}$ (13). Interstitial oxygen occupies a position away from the least crowded $(\frac{1}{4}, \frac{1}{4}, \frac{1}{4})$ lattice site; the short O–O separations present can be only rationalized if a neutral oxygen defect, not contributing to hole creation, is present.

Stoichiometric La_2CoO_4 is isostructural with La_2NiO_4 and La_2CuO_4, adopting the K_2NiF_4-type structure (14). However, Co^{2+} is extremely easily oxidized to Co^{3+} and studies in many laboratories have established that incorporation of excess oxygen readily occurs in the $La_2CoO_{4+\delta}$ system (15–18), especially when the reactions take place in air. Alternatively, the presence of La vacancies can also lead to formal Co oxidation states larger than +2 (19). In contrast to the corresponding Ni and Cu series, the cobaltates have not been comprehensively studied and the oxygen defect structure is as yet unknown. The stoichiometric compound adopts the orthorhombic *Bmab* structure at room temperature and shows a first-order transition to the tetragonal $P4_2/ncm$ structure at ≈ 135 K (14), in analogy with Ba-doped La_2CuO_4 (20). It has been also shown that doping La_2CuO_4 with small amounts of

[1] To whom correspondence should be addressed.

0022-4596/94 $6.00

Co leads to an unexpected reduction in the orthorhombic distortion (21). In this paper, we report high resolution powder neutron diffraction measurements on oxygen-rich single-phase $La_2Co_xCu_{1-x}O_{4+\delta}$ ($x = 0.25, 0.75$) solid solutions between 5 and 295 K. Models for the oxygen defect geometry are derived and compared with the earlier results on $La_2CuO_{4+\delta}$ and $La_2NiO_{4+\delta}$.

EXPERIMENTAL

In order to prepare samples with highly homogeneous dopant distributions, the solution-based citrate sol–gel technique was employed (6). Samples (10 g) of $La_2Co_xCu_{1-x}O_{4+\delta}$ ($x = 0.25, 0.75$) were prepared in this way. Firing temperatures of 650°C (24 hr), 950°C (48 hr in air, one intermediate regrind) and 1200°C (24 hr in a CO_2 flow, followed by slow cooling to room temperature) were employed for $La_2Co_{0.25}Cu_{0.75}O_{4+\delta}$. In the preparation of $La_2Co_{0.75}Cu_{0.25}O_{4+\delta}$, we employed firing temperatures of 650°C (24 hr in air) and 1150°C (24 hr in CO_2 flow). Phase purity of the samples was confirmed by powder X-ray diffraction, using a Siemens D-5000 diffractometer. The overall oxygen concentrations of the samples were determined by thermogravimetric reduction in flowing 95% Ar–5% H_2 using a Perkin-Elmer TGA-7 system. Samples (50 mg) were heated on a platinum pan to 850°C at a rate of 2.5°C/min (Fig. 1). Oxygen concentration was evaluated according to the reaction scheme:

$$La_2Co_xCu_{1-x}O_{4+\delta}\ (s) + (1 + \delta)\ H_2\ (g) \rightarrow La_2O_3\ (s) + xCo + (1 - x)Cu + (1 + \delta)H_2O\ (g) \quad [1]$$

The identity of the reaction products was confirmed by powder X-ray diffraction. Measurements were repeated more than once with consistent results. The oxygen excess in the Cu rich sample was estimated as $\delta = 0.10(2)$, while a substantially larger value was found for the Co rich sample, $\delta = 0.16(2)$. Thus the deduced compositions are $La_2Co_{0.25}Cu_{0.75}O_{4.10}$ and $La_2Co_{0.75}Cu_{0.25}O_{4.16}$. Figure 1 also shows a temperature plateau present in the weight-loss curve of the $x = 0.75$ sample (between 460 and 600°C), indicative of the existence of a formally stoichiometric sample $La_2Co_{0.75}Cu_{0.25}O_{3.99}$ in this temperature regime. The $x = 0.25$ sample shows no comparable plateau but only an inflexion point at ~430°C, corresponding to a formal stoichiometry of $La_2Co_{0.25}Cu_{0.75}O_{3.69}$. An identical oxygen content has been reported before (22) for the oxygen-deficient $La_2CuO_{3.67}$ system which was found to be isostructural with $Sr_2CuO_{3+\delta}$. Our results thus provide evidence that Co and possibly other divalent elements may be incorporated in the oxygen-rich $La_2CuO_{3.67}$ *S*-phase to form solid solutions.

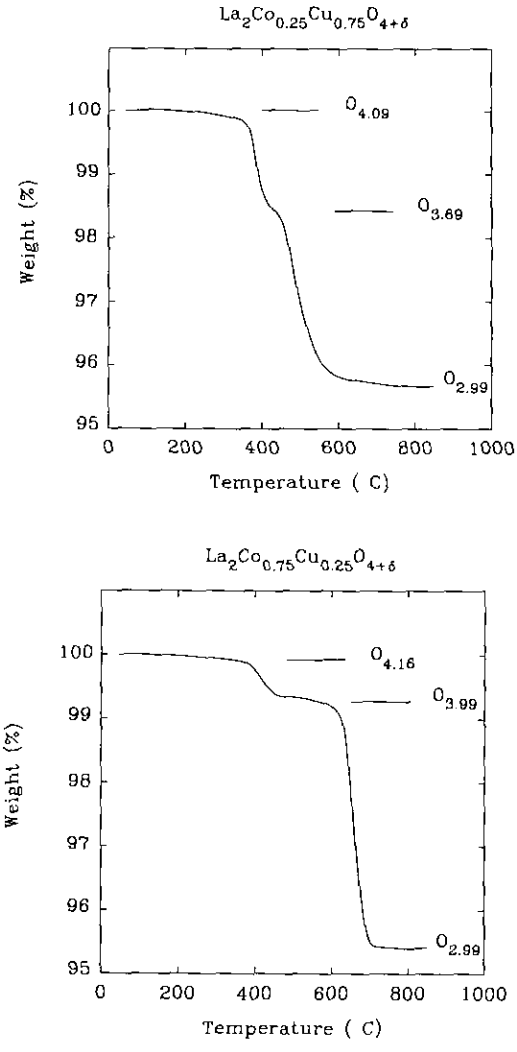

FIG. 1. Thermogravimetric reduction weight-loss curves for (a) $La_2Co_{0.25}Cu_{0.75}O_{4+\delta}$ and (b) $La_2Co_{0.75}Cu_{0.25}O_{4+\delta}$.

Powder neutron diffraction profiles of $La_2Co_{0.25}Cu_{0.75}O_{4.10}$ and $La_2Co_{0.75}Cu_{0.25}O_{4.16}$ were measured at various temperatures between 5 and 295 K on the D2b high-resolution powder diffractometer at the Institut Laue Langevin, Grenoble, using neutrons with a mean wavelength of 1.5946 Å. The instrument was operated in its high-intensity mode. The samples were mounted in cylindrical vanadium cans, placed in an ILL "orange" cryostat. Diffraction data were collected in steps (2θ) of 0.05°. A background cryostat run was also recorded in order to unravel the origin of weak diffraction features in the vicinity of 18°. The raw data were merged and, after background subtraction (23), profile refinements were performed by using the Rietveld profile method (24), and incorporating a pseudo-Voigt function peak shape description (25). The *d*-spacing range analyzed was 0.84–7.63 Å for both materials.

RESULTS

(a) *Profile Refinements of* $La_2Co_{0.25}Cu_{0.75}O_{4.10}$

Inspection of the diffraction profiles indicated symmetry lower than tetragonal at all temperatures; preliminary refinement of the profile recorded at the lowest temperature for this sample (50 K) using the standard *I4/mmm* space group of the K_2NiF_4-type structure resulted in unsatisfactory reliability factors, $R_{wp} = 0.262$ and $R_I = 0.086$. Indexing of the peaks was achieved in an enlarged orthorhombic unit cell with approximate dimensions $\sqrt{2}a \times \sqrt{2}a \times c$. Following earlier work on oxygen-rich $La_2CuO_{4+\delta}$ (10) and $La_2NiO_{4+\delta}$ (11) systems, we considered both the *Fmmm* and *Bmab* orthorhombic subgroups of *I4/mmm*. The *Fmmm* space group was found clearly inferior to *Bmab* since it failed in fitting a number of weak reflections ($2\theta \approx 21.87°$, 32.98°, 38.86°, 41.04°, 54.26°, 65.35°, 65.89°, 96.69°, and 106.38°) present in the profile. All these were nicely accounted for in the *Bmab* space group. Initial refinements, performed with the atoms in their normal lattice sites only, gave reliability factors, $R_{wp} = 0.126$ and $R_I = 0.074$ for *Fmmm* and $R_{wp} = 0.096$ and $R_I = 0.053$ for *Bmab*. The *Bmab* space group was consequently adopted in all subsequent refinements. The Cu and Co atomic positions and thermal parameters were constrained to be the same with their respective occupancies set at the expected stoichiometry and not further refined. When oxygen site occupancies were allowed to refine, no vacancy concentration was observed; values equal to 2.0, within the standard deviation, were obtained for both the apical, O(1), and the planar, O(2), oxygens.

We then started our search for the excess oxygen site, as necessitated by the thermogravimetric reduction results. For our preliminary model, we used a single-phase refinement in space group *Bmab* since no evidence of more than one phases present was apparent; however, we note that Jorgensen *et al.* (10, 11) find that for both the cuprate and nickelate systems, phase separation occurs for values of the oxygen excess $\delta \approx 0.09$, to an oxygen-rich *Fmmm* phase and a stoichiometric *Bmab* phase. No displacement of the apical oxygen from its normal site was initially applied and the oxygen defect model proposed by Morosin *et al.* (13) for the *Bmab* phase of $La_{1.84}Sr_{0.16}CuO_{4+\delta}$ was chosen at the starting point for our refinements. The oxygen interstitial defect, O(3), was introduced in the $(\frac{1}{4}, \frac{1}{4}, z; z \approx 0.162)$ position and the apical oxygen, O(1) was retained in its normal position $(\frac{1}{2}, y, z; y = -0.034, z = 0.180)$. The O(3) position was allowed to be displaced away from the $(\frac{1}{4}, \frac{1}{4}, \frac{1}{4})$ site along the long crystal axis *c* (Fig. 2). Satisfactory refinements were obtained fairly quickly. The positional parameter and occupancy of the defect converged to $z = 0.264(4)$ and $n(O(3)) = 0.109(8)$ with the isotropic temperature factor fixed at 1.0 Å^2. Reasonable thermal parameters were obtained for all the other atoms except for the apical oxygen which exhibited a large B_{iso} value of 1.68 Å^2; an anisotropic temperature factor was introduced for this atom and refined, leading to an improvement of the fit quality ($R_{wp} = 0.086$, $R_I = 0.038$).

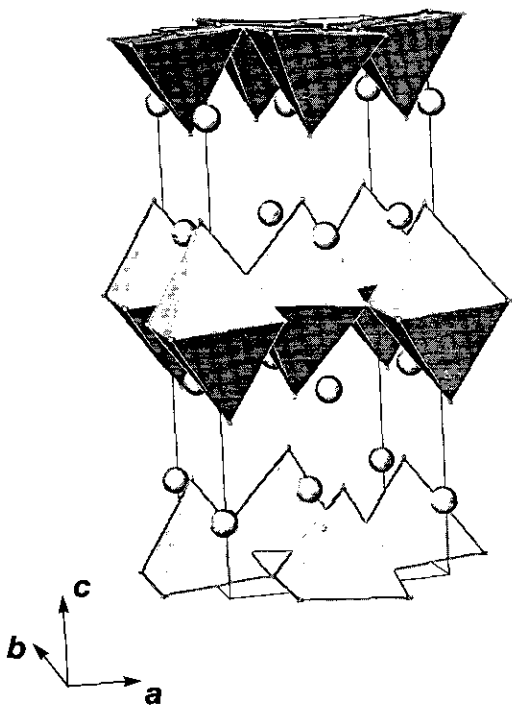

FIG. 2. The crystal structure of the stoichiometric La_2CuO_4 phase (orthorhombic space group *Bmab*).

Although the fit quality of these structural models suggest acceptable crystal structures for the $La_2Co_{0.25}Cu_{0.75}O_{4.10}$ material, a careful examination of the local environment of the oxygen defect revealed the presence of two very short O(1)–O(3) distances at 1.92(2) Å. This led us to investigate the possibility that some of the apical O(1) atoms might be displaced from their normal lattice sites to neighboring O(4) sites with coordinates (*x*, *y*, *z*), giving a more physically acceptable-local structure. The parameters of our earlier model with the apical oxygen at its normal lattice site were used as starting values. The starting position of the O(4) ion was that of Chaillout *et al.* (12) at (0.47, 0.10, 0.18), its isotropic thermal factor was set equal to the one of the apical oxygen O(1), $B \sim 1.6$ Å^2, and its site occupancy was constrained to satisfy $n(O(1)) + n(O(4)) = 2$. A step-by-step introduction of the various parameters to the fit led to stable refinements and an improved fit quality. Further improvement in the fit quality was achieved when an anisotropic temperature factor was refined for the equatorial O(2) atom (R_{wp} =

TABLE 1
Final Structural Parameters Derived from the Rietveld Profile Refinements

	$La_2Co_{0.75}Cu_{0.25}O_{4+\delta}$		$La_2Co_{0.25}Cu_{0.75}O_{4+\delta}$	
Space group	*Fmmm*		*Bmab*	
Temperature/K	5	295	50	295
a/Å	5.4548(2)	5.4638(3)	5.3857(1)	5.3972(1)
b/Å	5.4690(2)	5.4764(3)	5.4213(1)	5.4202(1)
c/Å	12.7465(4)	12.7847(5)	13.0096(3)	13.0512(3)
V/Å^3	380.262(25)	382.545(30)	379.851(17)	381.794(16)
x (La)	0	0	0.5	0.5
y	0	0	0.0081(5)	0.0061(8)
z	0.3609(1)	0.3609(2)	0.3618(1)	0.3616(1)
B/Å^2	0.73(3)	1.01(4)	0.57(2)	0.89(2)
x (Co/Cu)	0	0	0.5	0.5
$y = z$	0	0	0	0
B/Å^2	0.68(3)	0.83(4)	0.40(2)	0.70(2)
x (O(1))	0	0	0.5	0.5
y	0	0	−0.0332(5)	−0.0273(8)
z	0.1750(4)	0.1751(5)	0.1812(2)	0.1814(3)
B/Å^2	1.93(5)	2.27(7)	1.02(4)	1.24(4)
n	1.45(2)	1.46(3)	1.79(1)	1.67(1)
$x = y$ (O(2))	0.25	0.25	0.25	0.25
z	0	0	0.0066(3)	0.0034(6)
b_{11}	0.0081(10)	0.0093(14)	0.0024(5)	0.0027(5)
b_{22}	0.0013(5)	0.0029(12)	0.0068(5)	0.0116(7)
b_{33}	0.0029(2)	0.0031(2)	0.0013(1)	0.0024(2)
b_{12}	0.0000(5)	−0.0018(7)	0.0012(4)	0.0023(4)
n	2	2	2	2
$x = y$ (O(3))	0.25	0.25	0.25	0.25
z	0.230(2)	0.237(4)	0.269(3)	0.270(4)
B/Å^2	1.0	1.0	1.0	1.0
n	0.203(10)	0.180(12)	0.109(8)	0.101(8)
x (O(4))	−0.074(5)	−0.069(7)	0.408(6)	0.426(4)
y	−0.076(5)	−0.077(7)	0.067(5)	0.062(4)
z	0.171(1)	0.173(2)	0.187(3)	0.181(2)
B/Å^2	1.93(5)	2.27(7)	1.02(4)	1.24(4)
n	0.55(2)	0.54(3)	0.21(1)	0.33(1)
R_{wp}/% (R_e/%)	8.9(2.4)	9.4(3.9)	8.3(3.7)	8.2(3.6)
$R_{Mod(I)}$/% ($R^e_{Mod(I)}$/%)	3.0(1.6)	3.4(3.2)	3.4(2.4)	3.4(2.7)

0.083, R_I = 0.034). The O(4) position converged to (0.408(6), 0.067(5), 0.187(3)) with a partial occupancy of n(O(4)) ~ 0.21(1); this resulted in physically acceptable O(1)–O(3) distances (larger than ~1.92 Å, Table 2). The extra oxygen anions were now found at ($\frac{1}{4}$, $\frac{1}{4}$, z) with z = 0.269(3). The excess oxygen content of the oxide as deduced from the Rietveld refinement is δ = 0.109(8). This is in excellent agreement with the TGA determination of δ = 0.10(2). The final results are summarized in Table 1 and the observed, calculated and difference profiles (T = 50 K) are shown in Fig. 3.

In order to check for the uniqueness of the O(3)-defect position, a separate model refinement was also carried out with O(3) placed in the position ($\frac{3}{4}$, $\frac{3}{4}$, 0.269) which is not related by symmetry to ($\frac{1}{4}$, $\frac{1}{4}$, 0.269) in *Bmab*. The refinement again converged to the same position for O(3), namely ($\frac{3}{4}$, $\frac{3}{4}$, 0.231(4)), confirming its nature as a true minimum. The next step was to assume that the O-defect was distributed between two sites, i.e., O(3) at ($\frac{1}{4}$, $\frac{1}{4}$, 0.269) and O(3)′ at ($\frac{3}{4}$, $\frac{3}{4}$, 0.269). Refinement of the site occupancy was attempted without imposing any constraints. The refinement provided excellent evidence that the ($\frac{1}{4}$, $\frac{1}{4}$, 0.269) site is preferably occupied by the interstitial oxygen. After constraining the z coordinates to be equal and the thermal parameter for both sites constrained to B = 1.0 Å^2, refinement led to an occupancy of the O(3) site of 0.089(21) and of the O(3)′ site of 0.022(22). The reliability factors R_{wp} = 0.083 and R_I = 0.037 remained unchanged.

Diffraction data were also collected at 98, 146, 198, and 295 K. The same model was used successfully for profile

TABLE 2
Selected Bond Distances (Å) at Low Temperatures

Space Group	$La_2Co_{0.75}Cu_{0.25}O_{4.16}$ Fmmm	$La_2Co_{0.25}Cu_{0.75}O_{4.09}$ Bmab
Host Structure		
Co/Cu–O(1)	2.231(5) ×2	2.364(3) ×2
Co/Cu–O(2)	1.9311(0) ×4	1.9124(2) ×4
Mean	2.031(2)	2.063(1)
La–O(1)	2.369(5) ×1	2.360(3) ×1
	2.7656(8) ×2	2.987(4) ×1
		2.549(4) ×1
	2.7726(8) ×2	2.7537(7) ×2
La–O(2)	2.622(1) ×4	2.589(3) ×2
		2.662(3) ×2
Mean	2.659(1)	2.652(4)
O(1)–O(1)	3.330(4) ×2	3.248(4) ×2
	3.336(4) ×2	3.253(2) ×2
O(2)–O(2)	2.7274(0) ×2	2.6928(0) ×2
	2.7345(0) ×2	2.7162(4) ×2
O(1)–O(2)	2.951(4) ×4	3.028(4) ×2
		3.054(4) ×2
Defect Structure		
Co/Cu–O(4)	2.25(2)	2.51(4)
La–O(3)	2.25(2)	2.24(2)
	2.56(2)	2.58(3)
La–O(4)	2.34(3)	2.34(4)
	2.44(3)	2.33(3)
	2.49(2)	2.52(3)
O(1)–O(3)	2.28(2)	2.34(2)
O(3)–O(4)	2.63(3)	2.34(4)
	2.81(3)	2.58(3)

refinement at all temperatures. The room temperature refinement results are also included for comparison in Table 1. Figure 4a shows the temperature evolution of the lattice parameters. The long axis c expands smoothly with increasing temperature while the difference in the basal plane dimensions a and b becomes smaller, the orthorhombic strain decreasing smoothly from a value of $3.30(2) \times 10^{-3}$ at 50 K to $2.13(2) \times 10^{-3}$ at 295 K. Figure 5a presents the variation in the (Cu/Co)–O bond lengths with increasing temperature.

(*b*) *Profile Refinement of* $La_2Co_{0.75}Cu_{0.25}O_{4.16}$

Powder neutron diffraction profiles were collected at 5 K and at intermediate temperatures up to room temperature. Initial examination of the raw data at 5 K suggested that the pattern could be indexed again with an orthorhombic supercell of the tetragonal K_2NiF_4 structure ($a_O \sim b_O \sim \sqrt{2}a_T$, $c_O \sim c_T$). However, the orthorhombic distortion ($[(b - a)/(b + a)] \sim 1.30(4) \times 10^{-3}$) in the present material, which is characterized by a larger oxygen-excess present ($\delta \sim 0.16(2)$), is much smaller than the one found in $La_2Co_{0.25}Cu_{0.75}O_{4.10}$ ($3.30(2) \times 10^{-3}$); it is of the same order of magnitude as that of the oxygen-rich $La_2NiO_{4.18}$ system ($0.92(2) \times 10^{-3}$) (11). A structural model based on the tetragonal space group *I4/mmm* proved unsatisfactory since it predicted only a small number of the observed peaks. Similarly, the orthorhombic *Bmab* space group which we found appropriate for the $x = 0.25$ system, predicts peak intensities at 2θ positions where no Bragg reflections are present in the raw diffraction data. Thus an

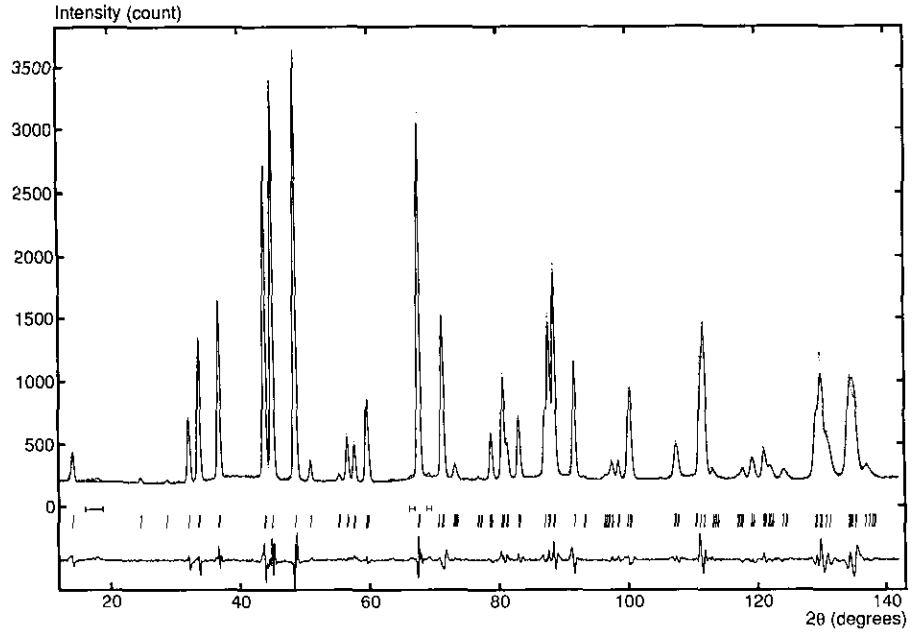

FIG. 3. Observed (points) and calculated (full curve) neutron diffraction profiles for $La_2Co_{0.25}Cu_{0.75}O_{4.09}$ at 50 K. The reflection markers and the difference profile are also shown. Scattering from the cryostat is also marked.

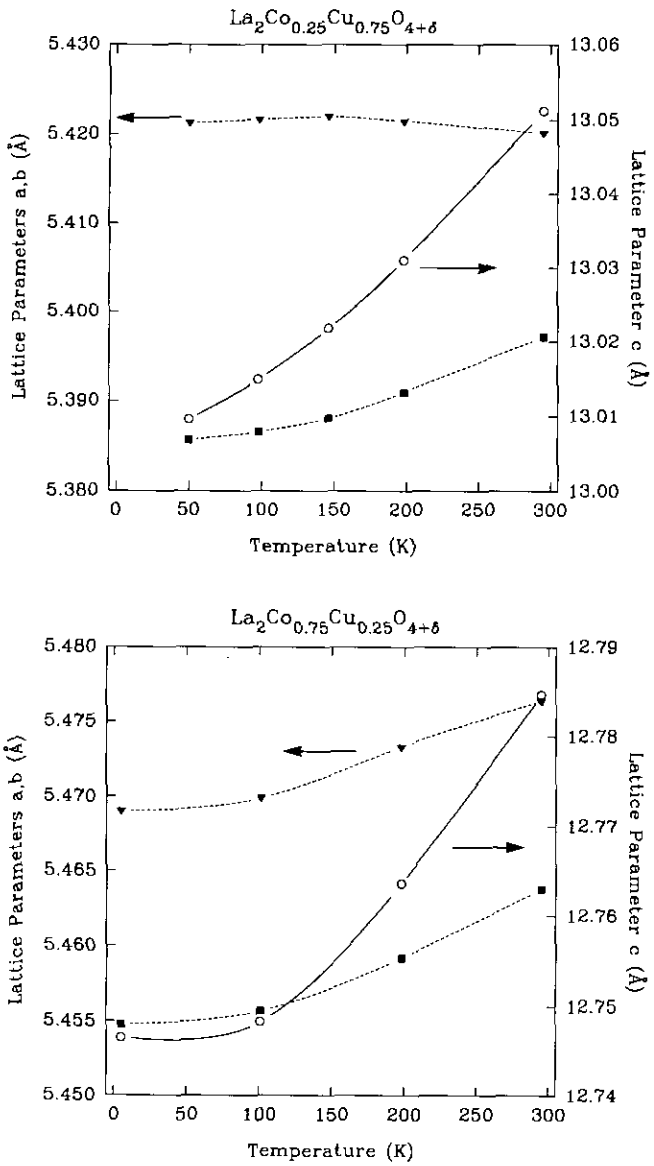

FIG. 4. Temperature evolution of the lattice constants of (a) $La_2Co_{0.25}Cu_{0.75}O_{4.10}$ and (b) $La_2Co_{0.75}Cu_{0.25}O_{4.16}$.

appropriate starting model was based on the orthorhombic *Fmmm* space group which was adopted for superoxygenated $La_2NiO_{4.18}$ (11).

Refinement with all atoms at the normal lattice sites of the *Fmmm* space group converged rapidly with reliability factors $R_{wp} = 0.132$, $R_I = 0.091$. However, this preliminary model with no oxygen excess led to unphysically large isotropic temperature factors for the apical oxygens (~3.2 Å^2). Such a situation had been encountered before (26) when excess interstitial ions (F^-) were present in the crystal structure of the T^* phases. In a similar fashion to $La_2NiO_{4.18}$ where the interstitial oxygen was located in the cavity present in the rock salt-like $(La_2O_2)^{2+}$ layers, it looks possible that a defect O(3) atom could occupy an analogous position in the $La_2Co_{0.75}Cu_{0.25}O_{4+\delta}$ unit cell. Such an oxygen defect will be coordinated to four apical oxygen O(1) anions and could lead to their displacement from their normal position along the c-axis. Such a displacement will manifest itself in unusually large thermal parameters in the undistorted structure.

Accordingly, a defect structural model was constructed with extra oxygen placed in an interstitial $(\frac{1}{4}, \frac{1}{4}, z)$ position with $z \sim 0.155$ and the apical O(1) oxygen split into two sites, with the displaced O(4) ions placed in a general symmetry position (x, y, z), with $x \sim -0.054$, $y \sim -0.118$, $z \sim 0.176$. The validity of such a defect model was also

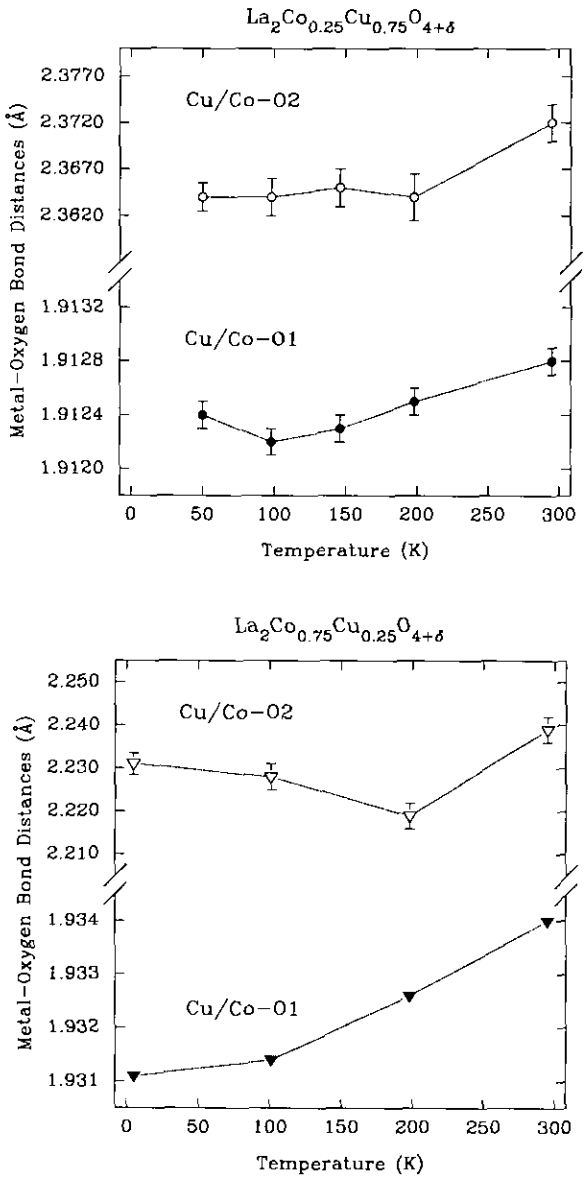

FIG. 5. Temperature evolution of the (Cu/Co)–O bond lengths in (a) $La_2Co_{0.25}Cu_{0.75}O_{4.10}$ and (b) $La_2Co_{0.75}Cu_{0.25}O_{4.16}$.

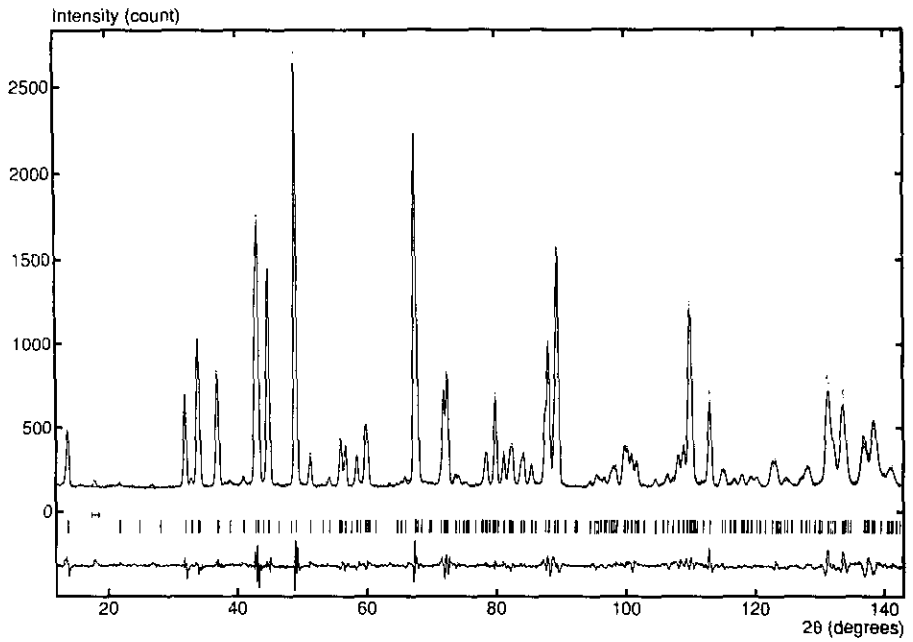

FIG. 6. Observed (points) and calculated (full curve) neutron diffraction profiles for $La_2Co_{0.75}Cu_{0.25}O_{4.16}$ at 5 K. The reflection markers and the difference profile are also shown. Scattering from the cryostat is also marked.

corroborated by the large vacancy concentration obtained for the apical O(1) oxygen when its site occupancy was refined while all the other atoms occupied their normal lattice sites in the *Fmmm* unit cell. In subsequent refinements, the site occupancies for O(1) and O(4) were constrained to satisfy the relationship $n(O(1)) + n(O(4)) = 2$, while the occupancy of the defect was fixed to $n(O(3)) \sim 0.2$. Even with these starting parameters, our model proved very stable, rapidly converging to $R_{wp} = 0.121$, $R_I = 0.075$, after refining fractional coordinates, isotropic temperature factors and occupancies for all the atoms in the unit cell, except the defect O(3). The fit quality was then significantly improved when the position of the interstitial oxygen defect was left free to vary. The refinement converged to $z(O(3)) \sim 0.234(3)$ with reliability factors $R_{wp} = 0.100$ and $R_I = 0.046$. We then allowed the site occupancy to vary. An unconstrained refinement rapidly converged, resulting in an oxygen excess of $\delta \sim 0.20(1)$, in excellent agreement with the value of $\delta \sim 0.16(2)$ independently determined by TGA. The use of anisotropic temperature factors to represent the thermal motion of the basal plane O(2) atoms further improved the agreement between the observed and calculated intensities ($R_I = 0.030$). The final parameters of the Rietveld profile refinement are also presented in Table 1 and the observed, calculated and difference profiles ($T = 5$ K) are shown in Figure 6.

Diffraction data were also collected at 101, 198, and 295 K. The same defect model in *Fmmm* was used successfully for profile refinement at all temperatures. The room temperature refinement results are also included for comparison in Table 1. Figure 4(b) shows the temperature evolution of the lattice parameters. All three axes expand smoothly with increasing temperature, the effect being more pronounced for the lattice constant c. The orthorhombic strain remains almost constant at $1.30(4) \times 10^{-3}$ to 200 K and then decreases only slightly to a value of $1.15(5) \times 10^{-3}$ at 295 K. Finally, Fig. 5(b) presents the variation in the (Cu/Co)–O bond lengths with increasing temperature.

DISCUSSION

In the present materials, the excess oxygen O(3) was introduced at sites located in the interstitial space defined by the rock salt-type La_2O_2 bilayers. In the $x = 0.75$ system, each O(3) is coordinated to four La and four O(1) atoms located at the (0, 0, 0.361) and (0, 0, 0.175) positions of the orthorhombic *Fmmm* unit cell, respectively and defining a "cube" (Fig. 7a). The defect is slightly displaced off the "center" ($\frac{1}{4}$, $\frac{1}{4}$, $\frac{1}{4}$) of the "cube" along the z axis so that $z = 0.230(2)$, and an occupancy of ~5% per formula unit. Its local environment consists of two short and two long La–O(3) distances at 2.247(15) Å and 2.557(20) Å, respectively, consistent with an O^{2-} defect. The presence of the excess oxygen, although it does not affect the (Cu, Co) coordination, causes a distortion of the (Cu, Co)O_6 octahedra. Some of the apical oxygen atoms O(1) are displaced from their normal lattice sites to a new site O(4) away from the [001] direction of the

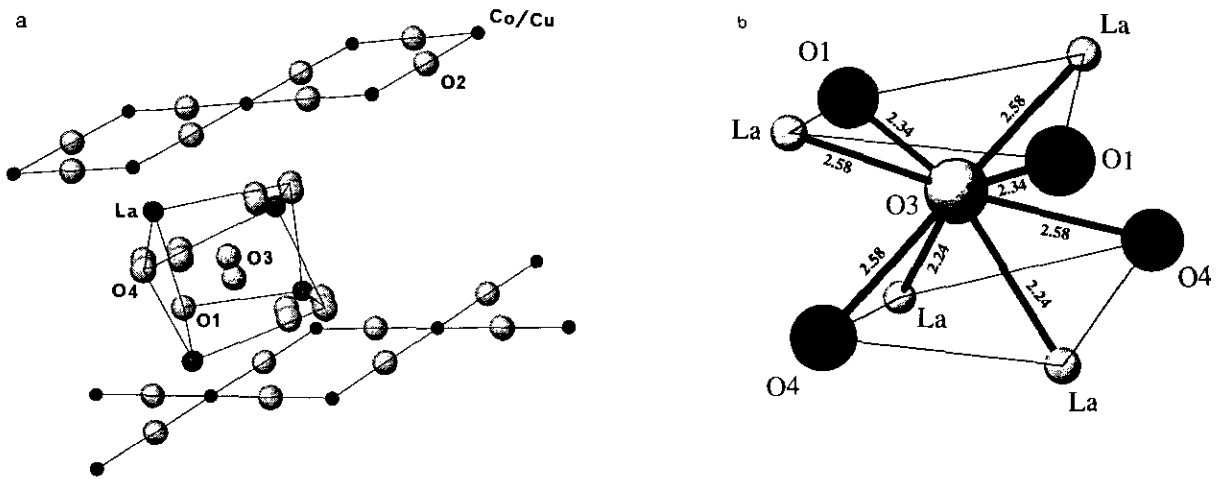

FIG. 7. (a) The coordination of the O(3) defect site in $La_2Co_{0.75}Cu_{0.25}O_{4.16}$ showing its splitting into two sites. The four possible symmetry-equivalent sites of the three displaced O(4) apical oxygens are also shown. The most likely coordination polyhedron ("cube") of the defect is drawn; the optimized O(3)–O(4) distances are 2.63(3) and 2.81(3) Å. (b) The defect O^{2-} local coordination in $La_2Co_{0.25}Cu_{0.75}O_{4.10}$ with bond distances given in Å.

Fmmm unit cell. As revealed by the refined ratio of the occupancy factors of the O(4) and O(3) atoms, n[O(4)] = 2.68(22) × n[O(3)], approximately *three* apical oxygens per formula unit are displaced for every O(3) interstitial site occupied. As a consequence, each O(3) atom is coordinated to three O(4) and one apical O(1) atoms. In the case of $La_2NiO_{4.18}$ (*11*), each O(3) defect was found to lead to the displacement of *four* neighboring O(1) atoms into O(4) sites. A list with the possible O(3)–O(1) and O(3)–O(4) distances is presented in Table 2. The possible O(3) environment, with only long, physically meaningful distances will involve one O(3)–O(1) distance at 2.28(2) Å and three O(3)–O(4) distances at 2.61(3) Å (×1) and 2.81(3) Å (×2) (Fig. 7a).

In the $La_2Co_{0.25}Cu_{0.75}O_{4.10}$ material, the excess oxygen is accommodated again in the same interstitial space ("cube") defined by the rock salt bilayers. The need of displacing the apical oxygen O(1) to the O(4) position becomes apparent because of the anomalously short interatomic distances encountered otherwise around the interstitial defect. Subsequent incorporation of the interstitial O^{2-} anions leads again to partially deformed CuO_6 octahedra, as approximately *two* apical oxygens per formula unit, n[O(4)] = 1.92(24) × n[O(3)] are displaced from their normal lattice site for each O(3) defect present. The coordination polyhedron of the interstitial anion O(3) has the shape of a "deformed" square antiprism with the extra oxygen coordinated to two short and two long La–O(3) distances at 2.24(2) Å and 2.58(3) Å, respectively. The rest of the corners of the polyhedron are occupied by two apical oxygens O(1) at 2.34(2) Å and two displaced O(4) ones at 2.58(3) Å, tetrahedrally positioned around the interstitial site. The O(3) defect is again displaced off-center along the long axis with z = 0.269(3) and an occupancy of ~5.5% per formula unit (Fig. 7b). Its position and occupancy are remarkably similar to the ones found for the x = 0.75 system; however, in the present case the O(3) atom is principally occupying only the ($\frac{1}{4}$, $\frac{1}{4}$, 0.269) site, while in $La_2Co_{0.75}Cu_{0.25}O_{4.16}$ it is equally shared between the symmetry-equivalent positions ($\frac{1}{4}$, $\frac{1}{4}$, 0.269) and ($\frac{1}{4}$, $\frac{1}{4}$, 0.231).

Gradual substitution of Cu by Co has a number of important structural consequences. The crystal chemistry and structural phase transitions of La_2CuO_4 have been discussed (3) in terms of the perovskite tolerance factors, $t = r_{Ln-O}/2^{1/2} r_{Cu-O}$ (27). Because of bond length mismatch between the lanthanide bilayers and the copper–oxygen layers, a tetragonal ($I4/mmm$) → orthorhombic ($Bmab$) phase transition occurs, characterized by the cooperative rigid tilting of the severely elongated CuO_6 octahedra about the [110] direction of the tetragonal unit cell. A strain displacement of the CuO_2 layers also occurs. A large orthorhombic distortion [$(b - a)/(b + a)$] ~7.61×10^{-3} results at low temperatures (3) with an octahedral tilt angle of 5.2(1)° and a basal plane strain angle (28) of 3.30(5)°. Partial substitution of the Jahn–Teller-active Cu^{2+} ion in the case of the $La_2Co_{0.25}Cu_{0.75}O_{4.10}$ material leads to reduced values for the orthorhombic distortion (~$3.29(2) \times 10^{-3}$), the metal–oxygen octahedral tilt angle (~4.4(1)°), and the elastic deformation of the basal plane (2.6(1)°). The tolerance factor t is still significantly smaller than 1 ($t \sim 0.91$) and the $Bmab$ space group is still adopted. Further substitution of the Cu^{2+} site leads to an increase in the tolerance factor towards the stability range of the tetragonal K_2NiF_4 structure and a further reduction of the orthorhombic distortion. In the Co-rich $La_2Co_{0.75}$

$Cu_{0.25}O_{4.16}$ material, the tolerance factor has increased to $t \sim 0.93$ and the orthorhombic distortion is found to be only $1.30(4) \times 10^{-3}$. Rigid tilts of the $(Cu,Co)O_6$ octahedra are no longer observed and the structure adopted is consistent with the face-centered *Fmmm* space group. The disorder present in the structure certainly contributes to the randomization of the rigid tilts which subsequently appear to average out, resulting in an orthorhombic structure with no strain displacement of the basal plane and no tilted octahedra. Finally, the Co-rich phase shows a greatly reduced average (c/a) ratio of 2.334 (cf., 2.408 for the Cu-rich sample) and less strongly elongated octahedra, $[(r_{ax} - r_{eq})/(r_{ax} - r_{eq})] = 0.072$ (cf., 0.106 for the Cu-rich sample), consistent with the decrease in the number of Jahn–Teller-active metal ions present.

CONCLUSIONS

We have presented high-resolution powder neutron diffraction structural measurements on $La_2Co_xCu_{1-x}O_{4+\delta}$ ($x = 0.25$, 0.75) samples containing a large excess of interstitial oxygen. The orthorhombic space group *Bmab*, resulting from alternate rigid tilting of the $(Co,Cu)O_6$ octahedra along the [110] direction of the tetragonal unit cell, describes the Cu-rich $x = 0.25$ orthorhombic phase well throughout the temperature range studied. No evidence for phase separation is found with the oxygen defect occupying a single "square antiprism" site within the lanthanide–oxygen bilayers and leading to the deformation of approximately two of its four neighboring octahedra. The orthorhombic strain is found to be highly reduced in the Co-rich $x = 0.75$ system which now adopts the face-centered *Fmmm* space group, as a result of the suppression of the tilting of the $(Co,Cu)O_6$ octahedra. The Jahn–Teller distortion of the octahedra is also found strongly reduced as a result of the substitution of Cu by Co. A related interstitial site is occupied by the defect leading to the deformation of approximately three of its four neighboring octahedra. In the present system, the defect splits between two symmetry-equivalent sites. In both oxides studied, the defect geometry is consistent with a negatively charged O^{2-} ion.

ACKNOWLEDGMENTS

We acknowledge financial support by the Science and Engineering Research Council (U.K.) and the European Economic Community (Brite-EURAM programme). Access to the neutron facilities at the Institut Laue Langevin, Grenoble, France is also gratefully acknowledged. We thank J. K. Cockcroft and G. Lüssem for help with the experiments.

REFERENCES

1. J. G. Bednorz and K. A. Müller, *Z. Phys. B* **64,** 189 (1986).
2. P. Day, M. J. Rosseinsky, K. Prassides, W. I. F. David, O. Moze, and A. K. Soper, *J. Phys. C* **20,** L429 (1987).
3. M. J. Rosseinsky, K. Prassides, and P. Day, *J. Mater. Chem.* **1,** 597 (1991).
4. H. Sawa, S. Suzuki, M. Watanabe, J. Akimitsu, K. Kolcirlo, H. Asaio, F. Izuki, and E. Takayama-Muromachi, *Nature* **337,** 347 (1989).
5. Y. Tokura, H. Takagi, and S. Uchida, *Nature* **337,** 345 (1989).
6. M. J. Rosseinsky, K. Prassides, and P. Day, *Physica C* **161,** 21 (1989).
7. M. J. Rosseinsky, K. Prassides, and P. Day, *Inorg. Chem.* **30,** 2680 (1991).
8. J. Beille, B. Chevalier, G. Demazeau, F. Deslandes, J. Etourneau, O. Laborde, C. Michel, P. Lejay, J. Provost, B. Raveau, A. Sulpice, J. L. Tholence, and R. Tournier, *Physica B* **146,** 307 (1987).
9. P. M. Grant, S. S. P. Parkin, V. Y. Lee, E. M. Engler, M. L. Ramirez, J. E. Vasquez, G. Lim, R. D. Jacowitz, and R. L. Greene, *Phys. Rev. Lett.* **58,** 2482 (1987).
10. J. D. Jorgensen, B. Dabrowski, S. Pei, D. G. Hinks, L. Soderholm, B. Morosin, J. E. Schirber, E. L. Venturini, and D. S. Ginley, *Phys. Rev. B* **38,** 11337 (1988).
11. J. D. Jorgensen, B. Dabrowski, S. Pei, D. R. Richards, and D. G. Hinks, *Phys. Rev. B* **40,** 2187 (1989).
12. C. Chaillout, S. W. Cheong, Z. Fisk, M. S. Lehmann, M. Marezio, B. Morosin, and J. E. Schirber, *Physica C* **158,** 183 (1989).
13. B. Morosin, G. H. Kwei, J. E. Schirber, J. A. Voigt, E. L. Venturini, and J. A. Goldstone, *Phys. Rev. B* **44,** 7673 (1991).
14. K. Yamada, M. Matsuda, Y. Endoh, B. Keimer, R. J. Birgeneau, S. Onodera, J. Mizusaki, T. Matsura, and G. Shirane, *Phys. Rev. B* **39,** 2336 (1989).
15. P. Lahuede and M. Daire, *C.R. Acad. Sci. (Paris) Ser. C* **276,** 1783 (1973).
16. J. J. Janecek and G. P. Wirtz, *J. Am. Ceram. Soc.* **61,** 242 (1978).
17. U. Lehmann and H. K. Müller-Buschbaum, *Z. Anorg. Allg. Chem.* **470,** 59 (1980).
18. R. A. Mohan Ram, P. Ganguly, and C. N. R. Rao, *Mater. Res. Bull.* **23,** 501 (1988).
19. J. T. Lewandowski, R. A. Beyerlein, J. M. Longo, and R. A. McCauley, *J. Am. Ceram. Soc.* **69,** 699 (1986).
20. J. D. Axe, A. H. Moudden, D. Hohlwein, D. E. Cox, K. M. Mohanty, A. R. Moodenbaugh, and Y. Xu, *Phys. Rev. Lett.* **62,** 2751 (1989).
21. A. Lappas, M. J. Rosseinsky, and K. Prassides, *Physica B* **165,** 1685 (1990).
22. F. C. Chou, J. H. Cho, L. L. Miller, and D. C. Johnston, *Phys. Rev. B* **42,** 6172 (1990).
23. A. W. Hewat, personal communication.
24. H. M. Rietveld, *J. Appl. Crystallogr.* **2,** 65 (1969).
25. J. K. Cockcroft, personal communication.
26. P. Lightfoot, S. Pei, J. D. Jorgensen, X. X. Tang, A Manthiram, and J. B. Goodenough, *Physica C* **169,** 15 (1990).
27. K. K. Singh, P. Ganguly, and C. N. R. Rao, *J. Solid State Chem.* **52,** 254 (1984).
28. J. P. Pouget, C. Noguera, and R. Moret, *J. Phys. (Paris)* **49,** 375 (1988).